catalysts

MDPI

Article

Facile Synthesis of N-Doped WS_2 Nanosheets as an Efficient and Stable Electrocatalyst for Hydrogen Evolution Reaction in Acidic Media

Arpan Kumar Nayak [1], Enhbayar Enhtuwshin [2], So Jung Kim [2] and HyukSu Han [2,*]

[1] Department of Physics: School of Advanced Sciences, Vellore Institute of Technology, Vellore 632014, India; aknayakju@gmail.com

[2] Department of Energy Engineering, Konkuk University, 120 Neungdong-ro, Gwangjin-gu, Seoul 05029, Korea; tuvshuu3388@gmail.com (E.E.); sjane9708@gmail.com (S.J.K.)

* Correspondence: hhan@konkuk.ac.kr; Tel.: +82-2-450-3997

Received: 30 September 2020; Accepted: 20 October 2020; Published: 26 October 2020

Abstract: Transition metal chalcogenides have been widely studied as a promising electrocatalyst for the hydrogen evolution reaction (HER) in acidic conditions. Among various transition metal chalcogenides, tungsten disulfide (WS_2) is a distinguishable candidate due to abundant active sites and good electrical properties. Herein, we report a facile and selective synthetic method to synthesize WS_2 with an intriguing two-dimensional nanostructure by using cysteine ($C_3H_7NO_2S$) as a chemical agent. In addition, nitrogen can be incorporated during chemical synthesis from cysteine, which may be helpful for enhancing the HER. The electrocatalytic activity of N-doped WS_2 exhibits a promising HER in acidic conditions, which are not only higher than $W_{18}O_{49}$ nanowires and hex-WO_3 nanowires, but also comparable to the benchmark Pt/C. Moreover, excellent electrocatalytic stability is also demonstrated for acidic HER during long-term tests, thus highlighting its potential use of practical applications as an electrolyzer.

Keywords: water splitting; hydrogen evolution reaction; electrocatalyst; tungsten sulfide

1. Introduction

Hydrogen is a promising future energy resource, which has the potential to replace fossil fuel stocks [1,2]. The electrochemical electrolyzer has become a crucial energy conversion system to produce hydrogen in a cost-effective and environmentally friendly way [3–5]. Compared to the conventional alkaline electrolyzer, the proton exchange membrane (PEM) electrolyzer has attracted great attention from researchers due to a much higher energy conversion efficiency. With this in mind, electrocatalysts for the hydrogen evolution reaction (HER) in acidic media becomes of paramount importance for efficient electrochemical water splitting using a PEM electrolyzer [6]. Noble metals such as Pt or Pd are currently marked as the best HER electrocatalysts in acidic media [7]. However, the scarcity and high cost of novel metals block their practical use. As such, low-cost electrocatalysts with a high performance need to be developed in order to replace the benchmark novel-metal-based electrocatalysts for the HER.

Tungsten-based compounds (i.e., chalcogenides or oxides) are reported as promising materials for acidic HER [8–10]. A multivalent W in the oxides or chalcogenides can give rise to a high probability of electrochemical reactions with electrochemical robustness in harsh acidic conditions. Especially, tungsten chalcogenides such as WS_x can exhibit promising electrocatalytic activity due to abundant active sites where both the metal and chalcogenide atoms are electrocatalytically active [11–16]. In addition, N dopants, possessing a high affinity to transition metals, can further enhance interfacial charge transfer in WS_x. The incorporated N atoms can modulate the local electronic structure of

transition metal atoms. Thus, water dissociation can be much more favorable in N-doped WS_x compared to the pristine WS_x, resulting in an enhanced HER [15].

In this context, here we report a facile synthetic method for N-doped WS_2 as a high-performance HER electrocatalyst in acidic media. Our chemical method could selectively synthesize WS_x or WO_x by simply changing chemical agents. In addition, an intriguing two-dimensional nanosheet structure was obtained for WS_2 with a successful incorporation of N via a one-step hydrothermal reaction using cysteine ($C_3H_7NO_2S$) as a chemical agent. The best sample showed a low overpotential of 130 mV for generating a current density of 10 mA cm^{-2} with excellent catalytic stability up to 12 h in 0.5 M H_2SO_4.

2. Results and Discussion

Figure 1 shows X-ray diffraction (XRD) patterns of $W_{18}O_{49}$, WO_3, WS_2 (cysteine 1:2, 0.01 M), and WS_2 (cysteine 1:4, 0.02 M). XRD results reveal that phase-pure $W_{18}O_{49}$ (JCPDS: 01-084-1516), WO_3 (JCPDS: 033-1387), and WS_2 (JCPDS: 008-0237) were successfully synthesized using our method. No secondary phases or impurities were presented for all samples. Notably, selective synthesis for each phase could be achieved by only adding thiourea or cysteine to the starting WCl_6 solution. This highlights the practical potential of our synthetic method for preparing tungsten-based compounds.

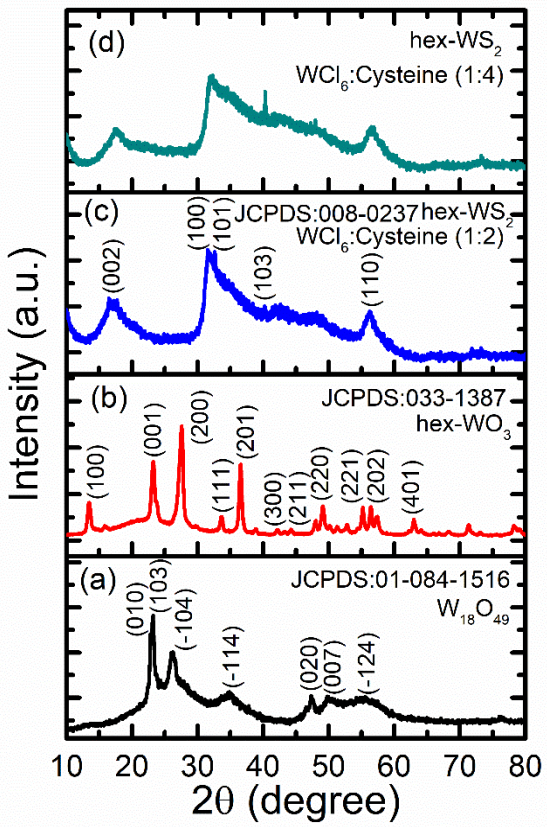

Figure 1. XRD patterns of (**a**) $W_{18}O_{49}$, (**b**) WO_3, (**c**) WS_2 (cysteine 1:2), and (**d**) WS_2 (cysteine 1:4).

SEM images of $W_{18}O_{49}$ are shown in Figure 2. A homogeneous nanowire morphology was observed for $W_{18}O_{49}$. A thickness on the order of a few tens of nanometers was observed for the $W_{18}O_{49}$, and no significant aggregation of nanowires occurred during the solvothermal synthesis (Figure 2b). After the addition of thiourea (CH_4N_2S) during the wet-chemical synthesis, a pristine nanowire morphology was well retained while the crystalline phase was changed from $W_{18}O_{49}$ to hexagonal WO_3 (Figure 3). With respect to the morphology, the nanowire thickness was slightly increased to about a few hundred nanometers for WO_3 compared to that of $W_{18}O_{49}$ (Figure 3b). Substantial changes in morphology occurred when cysteine ($C_3H_7NO_2S$) instead of thiourea (CH_4N_2S) was added to the

WCl_6 solution during wet-chemical synthesis (Figure 4). An intriguing nanoflower morphology was observed on the surface of the WS_2 nanoparticles (Figure 4b). The WS_2 (cysteine 1:2) nanoparticles showed a spherical shape with a diameter of about 300~500 nm. Interestingly, two-dimensional (2D) nanosheets with a thickness of a few nanometers were homogeneously grown on the surface of the WS_2 (cysteine 1:2) nanoparticle. For the WS_2 (cysteine 1:4) sample, a nearly identical morphology with WS_2 (cysteine 1:2) was observed (Figure 5), except that the particle size was slightly increased to about 500~700 nm. These results indicate that cysteine ($C_3H_7NO_2S$) in the starting WCl_6 solution can facilitate the formation of a tungsten sulfide phase (i.e., WS_2) in a 2D nanosheet structure during the hydrothermal reaction, whereas thiourea (CH_4N_2S) promotes the one-dimensional (1D) growth of tungsten oxide phases such as WO_3 or $W_{18}O_{49}$. Hence, a selective synthesis with phase and morphology control for tungsten-based nanomaterials can be realized via our simple and facile synthetic method. Notably, a well-defined 2D nanoflower morphology of WS_2 (cysteine 1:2) may be of importance for enhancing electrocatalytic activity due to the high surface area for electrochemical reactions.

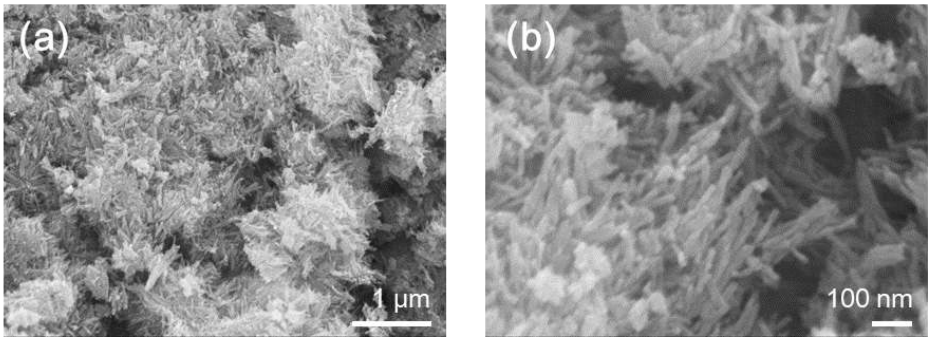

Figure 2. FESEM (**a**) low and (**b**) high resolution images of $W_{18}O_{49}$ nanowires synthesized using WCl_6 in ethanol at 180 °C for 24 h.

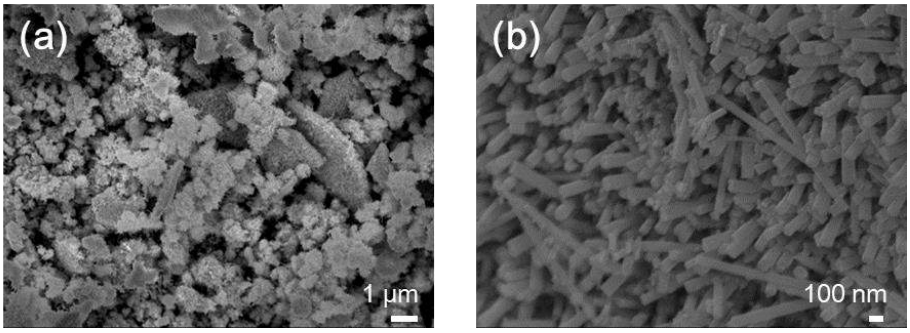

Figure 3. FESEM (**a**) low and (**b**) high resolution images of WO_3 nanowires synthesized using WCl_6 in ethanol and thiourea at 180 °C for 24 h.

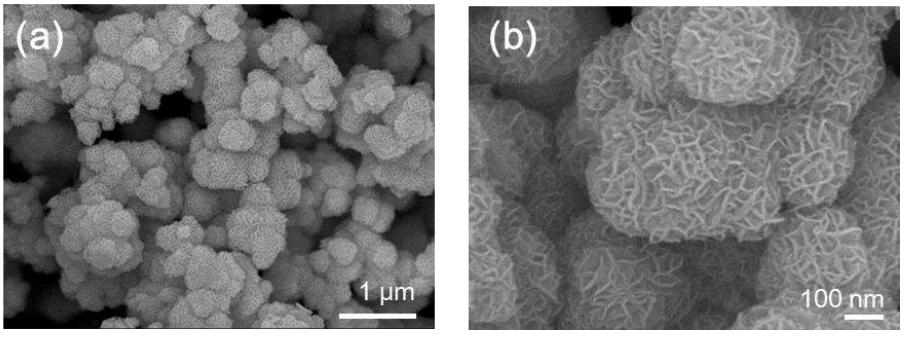

Figure 4. FESEM (**a**) low and (**b**) high resolution images of WS_2 nanosheets (cysteine 1:2) synthesized using WCl_6 in ethanol and cysteine at 180 °C for 24 h.

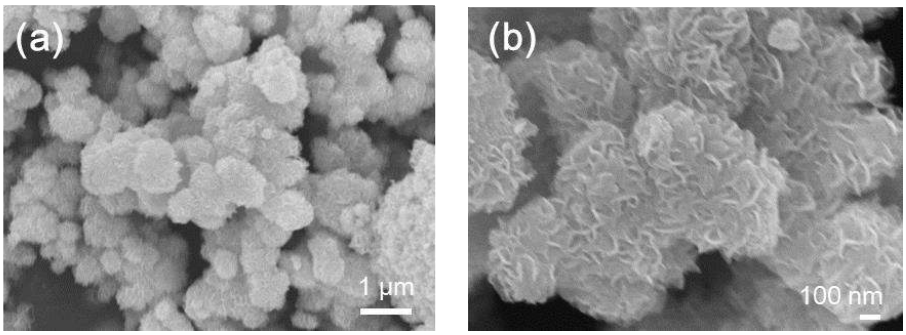

Figure 5. FESEM (**a**) low and (**b**) high resolution images of WS_2 nanosheets (cysteine 1:4) synthesized using WCl_6 in ethanol and cysteine at 180 °C for 24 h.

X-ray photoelectron spectroscopy (XPS) was performed on the WS_2 (cysteine 1:2) sample to study chemical and electronic structures of the surface (Figure 6). High-resolution XPS scans were measured on W 4f, S 2p, O 1s, and N 1s. The presence of W–S bonds in WS_2 (cysteine 1:2) was confirmed because W $4f_{3/2}$ and W $4f_{1/2}$ peaks were observed at 32.18 and 34.38 eV, respectively (Figure 6a) [14]. Two doublets were observed for W $4f_{3/2}$ and W $4f_{1/2}$ peaks, with the corresponding satellite peaks at 33.18 and 35.08 eV indicating the existence of W^{4+} in the hexagonal WS_2 phase. In the S 2p spectra, the XPS peaks for W–S were observed at ~161.88 eV (Figure 6b). The XPS peaks in the S 2p spectra near 163.18 and 164.68 eV are associated with S–O and S–OH bonds, respectively, which can be formed during solvothermal reaction using ethanol as a solvent [14]. The high-resolution XPS spectra of the O 1s core level is shown in Figure 6c. The prominent peak at binding energies of 531.78 eV can be ascribed to O–W^{6+} or O–W^{5+} bonds, respectively, which may be presented in the surface (oxy)hydroxide layers [6,17]. Notably, the high-resolution N 1s XPS spectra showed the presence of N in the WS_2 (cysteine 1:2) sample, which could have originated from cysteine ($C_3H_7NO_2S$) during the synthesis. The amount of nitrogen in the sample was determined as 2.41 at% by analyzing the relative peak area in the XPS spectrum. In addition, the deconvoluted N 1s peak revealed that the incorporated nitrogen is primarily present as quaternary nitrogen (~401.48 eV) with an additional sp2 hybridized nitrogen component (~399.8 eV). Given that pyridinic nitrogen can act as an active site for electrocatalytic reactions or promote charge transfer between the adsorbents and the catalyst surface, improved catalytic performance can be expected for the WS_2 (cysteine 1:2) sample owing to the pyridinic nitrogen [18–22].

The electrocatalytic HER performance of $W_{18}O_{49}$, WO_3, WS_2 (cysteine 1:2), and WS_2 (cysteine 1:4) was tested in 0.5 M H_2SO_4 solution using a three-electrode measurement system with a rotating disk electrode (RDE, glassy carbon) and a loading amount of 0.28 mg cm^{-2}. For comparison, the bare glassy carbon electrode (GCE) and the benchmark Pt/C (20 wt %) catalyst were also tested. Linear sweep voltammetry (LSV) was performed at a scan rate of 2 mV s^{-1} while the RDE was continuously rotated at 1600 rpm to remove any bubbles generated during the measurements. All the measured potentials were *iR*-compensated, which were then referenced to a reversible hydrogen electrode (RHE). Figure 7a shows LSV polarization curves for the measured samples. An overpotential to deliver −10 mA cm^{-2} (η_{10}) is widely used as a figure of merit to compare catalytic activity for the HER. Among the tested samples, the WS_2 (cysteine 1:2) sample exhibited the lowest η_{10} (130 mV), indicating its high electrocatalytic activity for the HER in acidic media, which is comparable to that of the benchmark Pt/C sample (80 mV). The η_{10} values of $W_{18}O_{49}$, WO_3, and WS_2 (cysteine 1:4) were determined as 233, 181, and 143 mV, respectively. Figure 7b shows the calculated Tafel slope for the tested samples. Notably, the Tafel slope of WS_2 (cysteine 1:2) (45 mV dec^{-1}) exhibited a much lower value compared to the control samples, except for Pt/C (31 mV dec^{-1}). This reveals that the WS_2 phase with a 2D nanosheet morphology is advantageous to obtain a superior electrocatalytic activity for the acidic HER compared to the $W_{18}O_{49}$ or WO_3 phases with a 1D nanowire morphology. Two major factors could be responsible for the superior electrocatalytic HER performance of the WS_2 (cysteine 1:4) and

(cysteine 1:2): (i) The higher electrical conductivity of the tungsten sulfide phase compared to the tungsten oxide phase can enhance charge transfer during the HER. (ii) A well-defined 2D nanosheet morphology can secure a high electrochemically active surface area for the HER. In addition, the higher catalytic activity of the WS_2 (cysteine 1:2) in comparison to the WS_2 (cysteine 1:4) can be attributed to the smaller particle size, leading to a higher surface area. The electrocatalytic stability of the WS_2 (cysteine 1:2) was tested using a chronoamperometric (CA) study. Additionally, the HER performance of WS_2 (cysteine 1:2) is compared with other recently reported catalysts based on transition metal chalcogenides in Table 1. The WS_2 (cysteine 1:2) showed outstanding HER performance in terms of low overpotential and the Tafel slope, highlighting its potential as a promising HER catalyst. Figure 7c presents CA data for the WS_2 (cysteine 1:2) sample for 10 h under the applied voltage of 0.14 V_{RHE} in 0.5 M H_2SO_4. Notably, no noticeable current decrease was observed during the CA test for 10 h. Moreover, the LSV polarization curve was also measured for the WS_2 (cysteine 1:2) sample after a continuous CA test for 10 h (Figure 7d). Almost identical LSV curves were obtained before and after the CA test. These results highlight the excellent electrocatalytic stability of the WS_2 (cysteine 1:2) sample for the HER in acidic conditions. These results demonstrate that the WS_2 (cysteine 1:2) can be a promising electrocatalyst with high activity and stability for the acidic HER. In addition, our facile synthetic method to simultaneously control materials' phases and nanostructures is of great significance for designing new functional catalytic nanomaterials.

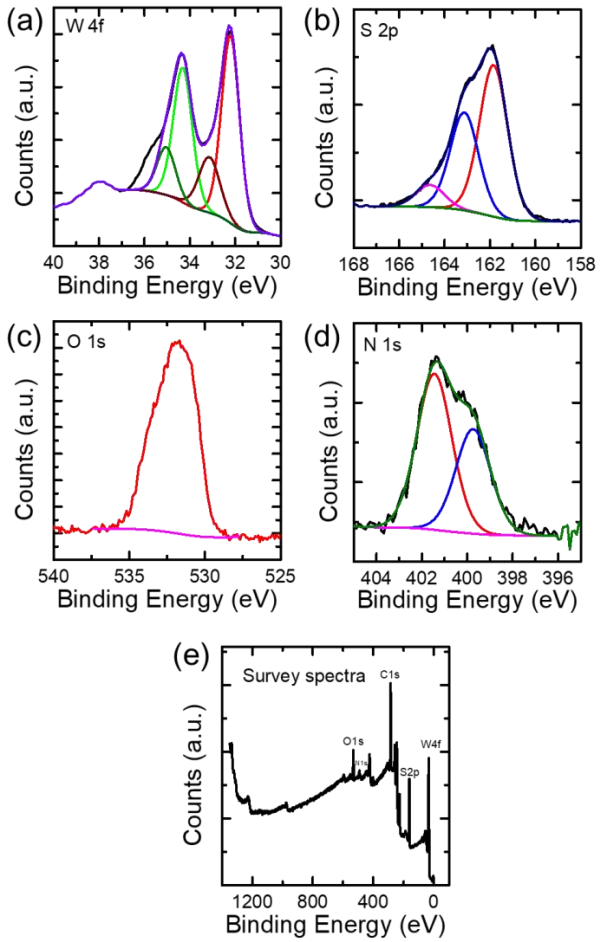

Figure 6. XPS spectra of WS_2 nanosheets (cysteine 1:2) for (**a**) W 4f, (**b**) S 2p, (**c**) O 1s, (**d**) N 1s, and (**e**) survey scan.

Table 1. Comparison of the catalytic HER properties by WS_2 (cysteine 1:2) to recently reported catalysts in 0.5 M H_2SO_4.

Materials	Overpotential (mV)	Tafel Slope (mV dec^{-1})	Reference
WS_2 (cysteine 1:2)	130 @ 10 mA cm^{-2}	45	This work
N-WS_2-H_2	197 @ 100 mA cm^{-2}	69	15
N-doped MoS_2	164 @ 10 mA cm^{-2}	71	19
Pd-WS_2 NF	175 @ 10 mA cm^{-2}	54	20
$V_{0.0065}$-WS_2/CC	148 @ 10 mA cm^{-2}	72	21
Te-doped WS_2	213 @ 10 mA cm^{-2}	94	22

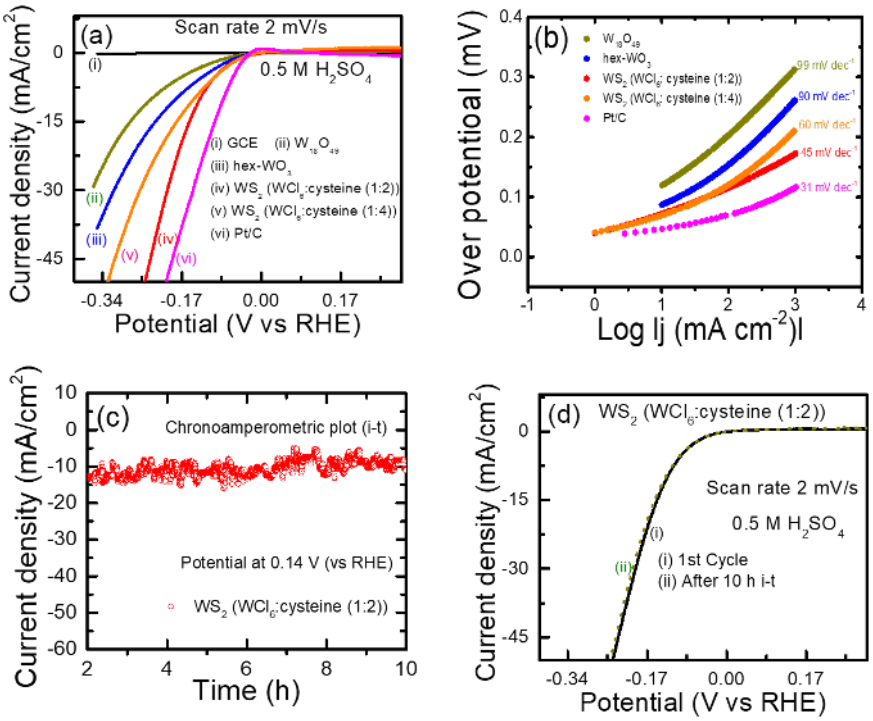

Figure 7. (**a**) Linear sweep voltammetry (LSV) polarization curves measured (*iR*-compensated) at a scan rate of 2 mV s^{-1} in 0.5 M H_2SO_4. (**b**) Calculated Tafel slopes of the samples. (**c**) CA curve of WS_2 nanosheets (cysteine 1:2) measured in 0.5 M H_2SO_4 for 10 h. (**d**) LSV curves of WS_2 nanosheets (cysteine 1:2) before and after the CA test. All current density is based on the geometric area of the electrode.

3. Experimental Procedure

3.1. Synthesis of $W_{18}O_{49}$ Nanowires

The material was synthesized using a solvothermal technique. In a typical synthesis, 0.005 M of WCl_6 (Sigma-Aldrich, St. Louis, MO, USA) was dissolved in 80 mL ethanol (Sigma-Aldrich, St. Louis, MO, USA) at room temperature and stirred for 30 min at a rotation speed of 400 rpm. The above solution was transferred to a 100 mL autoclave chamber. Then, the Teflon-linked stainless steel autoclave was heated at 180 °C for 24 h in a vacuum oven. The product was collected by centrifuging and washing several times using ethanol and distilled water. Finally, the sample was dried at 60 °C overnight in a hot air oven.

3.2. Synthesis of Hex-WO_3 Nanowires

During the synthesis of $W_{18}O_{49}$, 0.01 M of thiourea (CH_4N_2S, Sigma-Aldrich, St. Louis, MO, USA) was added to the WCl_6-ethanol solution and stirred for 30 min with a rotation speed of 400 rpm at room temperature. Then the Teflon-lined stainless-steel autoclave was heated at 180 °C for 24 h in a vacuum oven. The blue-colored precipitate powder was collected by centrifuging and washing several times using ethanol and distilled water. Finally, the sample was dried at 60 °C overnight in a hot air oven.

3.3. Synthesis of Hex-WS_2 Nanosheets

During the synthesis of hex-WO_3, 0.01 M and 0.02 M of cysteine ($C_3H_7NO_2S$, Sigma-Aldrich, St. Louis, MO, USA) was used by replacing thiourea (CH_4N_2S), keeping rest of the parameters fixed. The black-colored precipitate powder was collected by centrifuging and washing several times using ethanol and distilled water. Finally, the sample was dried at 60 °C overnight in a hot air oven.

3.4. Structural and Chemical Characterizations

An X-ray diffractometer (XRD, D/MAX RINT-2000, Rigaku, Tokyo, Japan) was employed to investigate the crystal structures of the samples using Cu Kα X-rays (1.54 Å) at 40 kV and 40 mA. Field-emission scanning electron microscopy (FE-SEM, JSM-7600F, Jeol, Tokyo, Japan) was used to study the morphology of the samples. The electronic structure and valence states of the samples were analyzed by X-ray photoelectron spectroscopy (XPS, Thermo Scientific K-Alpha$^+$, Thermo Fisher Scientific, Waltham, MA, USA) with 100 and 20 eV for the XPS survey and high-resolution scans, respectively.

3.5. Electrochemical Characterization

The electrochemical properties of the samples were studied using a standard three-electrode system (Autolab PGSTAT, Metrohm Autolab, Utrecht, Netherlands). A rotating disk electrode (RDE, Meetrohm Autolab, Utrecht, Netherlands) configuration was used for all electrochemical tests. A 0.5 M H_2SO_4 electrolyte was used for the electrochemical tests. A quantity of 5 mg of the catalyst powder was mixed well in a solution of 1 mL of water and ethanol with a volume ratio of 3:1. A Nafion® solution (5 wt %, 30 μL, Sigma-Aldrich, St. Louis, MO, USA) was added to secure a rigid bind between catalyst powder and the electrode surface. Five microliters of as-prepared catalyst ink was drop-coated on the glassy carbon (GC) RDE electrode with a diameter of 3 mm. Then, the electrode was dried overnight at room temperature. The RDE electrode as the working electrode, Ag/AgCl (3.0 M KCl, Meetrohm Autolab, Utrecht, Netherlands) as the reference electrode, and graphite rod as the counter electrode were used for all electrochemical tests. Voltage calibration was performed to change the measured working potential to the reversible hydrogen electrode (RHE). A scan rate of 2 mV s^{-1} was used for the linear sweep voltammetry.

4. Conclusions

$W_{18}O_{49}$, WO_3, WS_2 (cysteine 1:2), and WS_2 (cysteine 1:4) were synthesized via a one-step facile solvothermal method. The phase-selective synthesis was achieved by simply changing starting precursors such as cysteine ($C_3H_7NO_2S$) or thiourea (CH_4N_2S). XRD and SEM results confirm that cysteine ($C_3H_7NO_2S$) facilitates the formation of tungsten sulfide phases in a 2D nanosheet morphology, while thiourea (CH_4N_2S) promotes the formation of tungsten oxide phases in a 1D nanowire structure. The electrocatalytic activity of the samples was tested for the acidic HER, and the WS_2 (cysteine 1:2) showed the best catalytic performance among the tested samples, comparable to that of the benchmark Pt/C catalyst. In addition, excellent electrocatalytic stability was demonstrated for the WS_2 (cysteine 1:2) using a long-term stability test. These results reveal that our facile chemical synthetic method is powerful for the design of high-performance electrocatalysts with controlled phase and morphology.

Author Contributions: Conceptualization, A.K.N. and H.H; methodology, H.H.; formal analysis, E.E. and S.J.K.; investigation, A.K.N.; writing—original draft preparation, A.K.N. and H.H.; writing—review and editing, H.H.;

supervision, A.K.N. and H.H.; project administration, A.K.N. and H.H.; funding acquisition, A.K.N. and H.H. All authors have read and agreed to the published version of the manuscript

Funding: This research received no external funding.

Acknowledgments: We thank for Heejun Chung for fruitful discussions on this work.

Conflicts of Interest: The authors declare no conflict of interest.

References

1. Faisal, F.; Stumm, C.; Bertram, M.; Waidhas, F.; Lykhach, Y.; Cherevko, S.; Xiang, F.; Ammon, M.; Vorokhta, M.; Šmíd, B.; et al. Electrifying model catalysts for understanding electrocatalytic reactions in liquid electrolytes. *Nat. Mater.* **2018**, *17*, 592–598. [CrossRef] [PubMed]
2. Stamenkovic, V.R.; Strmcnik, D.; Lopes, P.P.; Markovic, N.M. Energy and fuels from electrochemical interfaces. *Nat. Mater.* **2016**, *16*, 57–69. [CrossRef] [PubMed]
3. Bonaccorso, F.; Colombo, L.; Yu, G.; Stoller, M.; Tozzini, V.; Ferrari, A.C.; Ruoff, R.S.; Pellegrini, V. Graphene, related two-dimensional crystals, and hybrid systems for energy conversion and storage. *Science* **2015**, *347*, 1246501. [CrossRef] [PubMed]
4. Chu, S.; Cui, Y.; Liu, N. The path towards sustainable energy. *Nat. Mater.* **2016**, *16*, 16–22. [CrossRef]
5. Han, H.; Choi, H.; Mhin, S.; Hong, Y.-R.; Kim, K.M.; Kwon, J.; Ali, G.; Chung, K.Y.; Je, M.; Umh, H.N.; et al. Advantageous crystalline–amorphous phase boundary for enhanced electrochemical water oxidation. *Energy Environ. Sci.* **2019**, *12*, 2443–2454. [CrossRef]
6. Han, H.; Nayak, A.K.; Choi, H.; Ali, G.; Kwon, J.; Choi, S.G.; Paik, U.; Song, T. Partial Dehydration in Hydrated Tungsten Oxide Nanoplates Leads to Excellent and Robust Bifunctional Oxygen Reduction and Hydrogen Evolution Reactions in Acidic Media. *ACS Sustain. Chem. Eng.* **2020**, *8*, 9507–9518. [CrossRef]
7. Cheng, N.; Stambula, S.; Wang, D.; Banis, M.N.; Liu, J.; Riese, A.; Xiao, B.; Li, R.; Sham, T.-K.; Liu, L.-M.; et al. Platinum single-atom and cluster catalysis of the hydrogen evolution reaction. *Nat. Commun.* **2016**, *7*, 13638. [CrossRef]
8. Song, S.; Guo, M.; Zhang, S.; Zhan, K.; Yan, Y.; Yang, J.; Zhao, B.; Xu, M. Plasma-assisted synthesis of hierarchical NiCoxPy nanosheets as robust and stable electrocatalyst for hydrogen evolution reaction in both acidic and alkaline media. *Electrochim. Acta* **2020**, *331*, 135431. [CrossRef]
9. Ma, B.; Yang, Z.; Chen, Y.; Yuan, Z.-H. Nickel cobalt phosphide with three-dimensional nanostructure as a highly efficient electrocatalyst for hydrogen evolution reaction in both acidic and alkaline electrolytes. *Nano Res.* **2018**, *12*, 375–380. [CrossRef]
10. Shan, S.J.; Ling, T.; Davey, K.; Zheng, Y.; Qiao, S. Transition-Metal-Doped RuIr Bifunctional Nanocrystals for Overall Water Splitting in Acidic Environments. *Adv. Mater.* **2019**, *31*, e1900510. [CrossRef]
11. Xu, K.; Wang, F.; Wang, Z.; Zhan, X.; Wang, Q.; Cheng, Z.; Safdar, M.; He, J. Component-Controllable $WS_{2(1-x)}Se_{2x}$ Nanotubes for Efficient Hydrogen Evolution Reaction. *Acs Nano* **2014**, *8*, 8468–8476. [CrossRef]
12. Lukowski, M.A.; Daniel, A.S.; English, C.R.; Meng, F.; Forticaux, A.; Hamers, R.J.; Jin, S. Highly active hydrogen evolution catalysis from metallic WS_2 nanosheets. *Energy Environ. Sci.* **2014**, *7*, 2608–2613. [CrossRef]
13. Tsai, C.; Chan, K.; Abild-Pedersen, F.; Nørskov, J.K. Active edge sites in $MoSe_2$ and WSe_2 catalysts for the hydrogen evolution reaction: A density functional study. *Phys. Chem. Chem. Phys.* **2014**, *16*, 13156–13164. [CrossRef]
14. Tan, S.M.; Pumera, M. Bottom-up Electrosynthesis of Highly Active Tungsten Sulfide (WS_{3-x}) Films for Hydrogen Evolution. *Acs Appl. Mater. Interfaces* **2016**, *8*, 3948–3957. [CrossRef]
15. Sun, C.; Zhang, J.; Ma, J.; Liu, P.; Gao, D.; Tao, K.; Xue, D. N-doped WS_2 nanosheets: A high-performance electrocatalyst for the hydrogen evolution reaction. *J. Mater. Chem. A* **2016**, *4*, 11234–11238. [CrossRef]
16. Anurupa, M.; Suneel, K.S. Sulphur edge and vacancy assisted nitrogen–phosphorus co-doped exfoliated tungsten disulfide: A superior electrocatalyst for hydrogen evolution reaction. *J. Mater. Chem A* **2018**, *6*, 19712–19726.
17. Bai, S.; Zhang, K.; Wang, L.; Sun, J.; Luo, R.; Li, D.; Chen, A. Synthesis mechanism and gas-sensing application of nanosheet-assembled tungsten oxide microspheres. *J. Mater. Chem. A* **2014**, *2*, 7927–7934. [CrossRef]

18. Bin Yang, H.; Miao, J.; Hung, S.-F.; Chen, J.; Tao, H.B.; Wang, X.; Zhang, L.; Chen, R.; Gao, J.; Chen, H.M.; et al. Identification of catalytic sites for oxygen reduction and oxygen evolution in N-doped graphene materials: Development of highly efficient metal-free bifunctional electrocatalyst. *Sci. Adv.* **2016**, *2*, e1501122. [CrossRef]
19. Van-Truong, N.; Yang, T.-Y.; Le, P.A.; Yen, P.-J.; Chueh, Y.-L.; Wei, K.-H. New Simultaneous Exfoliation and Doping Process for Generating MX_2 Nanosheets for Electrocatalytic Hydrogen Evolution Reaction. *ACS Appl. Mater. Interfaces.* **2019**, *11*, 14786–14795.
20. Amirohossein, H.; Nguyen, T.P.; Tekalgne, M.; Le, Q.V.; Choi, K.S.; Lee, T.H.; Park, T.J.; Kim, S.Y.; Jang, H.W. The role of metal dopants in WS_2 nanoflowers in enhancing the hydrogen evolution reaction. *Appl. Catal. A Gen.* **2018**, *567*, 73–79.
21. Anning, J.; Zhang, B.; Li, Z.; Jin, G.; Hao, J. Vanadium-Doped WS_2 Nanosheets Grown on Carbon Cloth as a Highly Efficient Electrocatalyst for the Hydrogen Evolution Reaction. *Chem. Asian J.* **2018**, *13*, 1438–1446.
22. Pan, Y.; Zheng, F.; Wang, X.; Qin, H.; Liu, E.; Sha, J.; Zhao, N.; Zhang, P.; Ma, L. Enhanced electrochemical hydrogen evolution performance of WS_2 nanosheets by Te doping. *J. Catal.* **2020**, *382*, 204–211. [CrossRef]